Full Title: High affinity Na^+ transport by wheat HKT1;5 is blocked by K^+

Running title: HKT1;5 proteins catalyse dual affinity Na^+ transporter in wheat

Authors: Bo Xu[1,2], Maria Hrmova[2] and Matthew Gilliham[1,2*]

[1]Australian Research Council Centre of Excellence in Plant Energy Biology, University of Adelaide, Waite Research Precinct, Glen Osmond, South Australia 5064, Australia

[2]School of Agriculture, Food and Wine, and Waite Research Institute, University of Adelaide, Waite Research Precinct, Glen Osmond, South Australia 5064, Australia

[*]Corresponding author: e-mail: matthew.gilliham@adelaide.edu.au

Keywords: salinity; High-affinity K Transporters; membrane transport; KtrB; dual affinity; sodium exclusion

Abstract

The wheat sodium transporters TmHKT1;5-A and TaHKT1;5-D are encoded by genes underlying major shoot Na^+ exclusion loci *Nax2* and *Kna1* from *Triticum monococcum* (Tm) and *Triticum aestivum* (Ta), respectively. In contrast to HKT2 transporters that have been shown to exhibit high affinity K^+-dependent Na^+ transport, HKT1 proteins have, with one exception, only been shown to catalyse low affinity Na^+ transport and no K^+ transport. Here, using heterologous expression in *Xenopus laevis* oocytes we show that both TmHKT1;5-A and TaHKT1;5-D encode dual (high and low) affinity Na^+-transporters with the high-affinity component being abolished when external K^+ is in excess of external Na^+. Based on 3-D structural modelling we propose that tighter binding of K^+, compared to that of Na^+ in the selectivity filter region by means of additional van der Waals forces, explains the K^+ block at the molecular level. The low-affinity component for Na^+ transport of TmHKT1;5-A had a lower K_m than that of TaHKT1;5-D and was less sensitive to external K^+. We propose that these properties underpin the improvements in shoot Na^+-exclusion and crop plant salt tolerance following the introgression of TmHKT1;5-A into diverse wheat backgrounds.

39 **Introduction**

40 Crops suffer reduced growth and productivity under salinity stress. Salt, when it
41 builds up to high concentrations in the growing medium (i.e. soil solution) imposes an
42 osmotic limitation on water uptake, interferes with optimal nutrient homeostasis, and
43 leads to the build up of leaf cellular sodium (Na^+) concentrations, which causes an
44 ionic toxicity that limits photosynthesis and carbon assimilation in plants (1).
45
46 A major genetic mechanism contributing towards salinity tolerance of most crops
47 including the cereals rice (*Oryza sativa*) and wheat (*Triticum aestivum* and *Triticum*
48 *monococcum*) is Na^+ exclusion from leaves, with the High-affinity potassium (K^+)
49 transporter (HKT) protein family having a major role in this trait (2-6). This family of
50 proteins is present in all plants so far sequenced; more broadly the members of the
51 high affinity K^+/Na^+ transporting Ktr/TrK/HKT superfamily of proteins are present in
52 bacteria (Ktr and TrK), fungi (TrK) and plants (HKT) (7,8).
53
54 These plant HKTs are divided into 2 clades: 1) class 1 HKT proteins (HKT1;x) are
55 mostly Na^+-selective transporters; 2) whereas class 2 HKTs (HKT2;y) mostly function
56 as K^+-Na^+ symporters and so far have been only identified in cereal monocots (9,10).
57 This definition has been challenged on occasion, such as for OsHKT2;4, where
58 following its characterization in *Xenopus laevis* oocytes, there are conflicting reports
59 on its permeability to Ca^{2+}, Mg^{2+} and NH_4^+ in addition to K^+ and Na^+ (11-13).
60 Furthermore, there are two reports of K^+ permeability in the HKT1 clade. Firstly,
61 *Arabidopsis* AtHKT1 could complement K^+ transport deficient *E. coli,* although no
62 K^+ permeability could be found when *AtHKT1* was expressed in *X. laevis* oocytes in
63 the same study (14). Secondly, *Eucalyptus camaldulensis* EcHKT1;1 and EcHKT1;2,
64 which appear to be the exception for the HKT1 proteins characterized so far in that
65 they transport both Na^+ and K^+ when expressed in *X. laevis* oocytes (15). Other HKT1
66 transporters have no reported K^+ permeability (4,5,10,14,16-20).
67
68 Whilst K^+ transport is not a common feature of HKT1 transporters, several have
69 shown the property of K^+-regulated Na^+ transport (19,21-23). For instance, the
70 presence of 10 mM external K^+ ($[K^+]_{ext}$) reduced the inward Na^+ current of *X. laevis*
71 oocytes expressing *HKT1;5* from *T. aestivum* (*TaHKT1;5-D*) (19), and reduced
72 outward Na^+ currents generated by expression of *HKT1;2* from *Solanum*

73 *lycopersicum* (*SlHKT1;2*) (21). Interestingly, $[K^+]_{ext}$ stimulated both inward and
74 outward Na^+ transport of *X. laevis* oocytes expressing two *HKT1;4* alleles from
75 *Triticum turgidum* L. subsp. *Durum*, when assayed with solutions of very low ionic
76 strength (23).
77
78 Ktr/TrK/HKT proteins are predicted to consist of 8 transmembrane α-helices that fold
79 into four pseudo-tetramers around a central pore (6,16,18). The selectivity filter lining
80 the pore of Ktr and TrK and class 2 HKT proteins is composed of four glycine
81 residues. In class 1 HKTs the first glycine within the predicted selectivity filter is
82 substituted with serine (16); the lack of K^+ permeability in this clade has been linked
83 to the presence of this glycine substitution (glycine for serine) (10,14,16-18); but the
84 exact molecular mechanism underlying this block is to be determined.
85
86 Here, we further characterise HKT1;5 proteins underlying two major salt tolerance
87 associated loci, *TmHKT1;5-A* (*Nax2*) and *TaHKT1;5-D* (*Kna1)* from *T. monococcum*
88 *and T. aestivum* respectively. We find that both TmHKT1;5-A and TaHKT1;5-D
89 encode dual affinity Na^+-transporters and that their dual affinity Na^+ transport can be
90 blocked by raising the external K^+ concentration. We further propose that the
91 adjoining residues within the selectivity filter cause this block by the virtue of a
92 higher number of van der Waals interactions with the K^+ ion, than with Na^+. Thus, the
93 Na^+ ion is capable of traversing the selectivity filter, while K^+ causes a block. This is
94 the first report that Na^+ transport has two affinities in the HKT1 clade and
95 demonstrates that dual affinity transport is a common property of both clades of the
96 HKT family.
97
98 **Results**
99 **K^+ sensitivity of TmHTK1;5-A and TaHKT1;5-D**
100 Previously, it was shown that inward Na^+ transport of both TmHKT1;5-A and
101 TaHKT1;5-D was inhibited by external K^+ ($[K^+]_{ext}$) (4,19). Here, we further compared
102 the K^+-sensitivity of TmHKT1;5-A and TaHKT1;5-D (Fig. 1). An increase in $[K^+]_{ext}$
103 to 30 mM reduced the channel inward conductance (i.e. <100 mV) of TmHKT1;5-A
104 by approximately 75% in a 1 mM Na^+ ($[Na^+]_{ext}$) bath solution; similarly this amount
105 of K^+ inhibited that of TaHKT1;5-D up to 95 % (Figs. 1A, 1B and 2). However, such
106 Na^+-inhibition by K^+ was gradually decreased by increasing $[Na^+]_{ext}$ (Figs. 1 and 2).

107 For instance, 10 mM $[K^+]_{ext}$ suppressed the channel inward conductance of
108 TmHKT1;5-A by 43.5% in 1 mM $[Na^+]_{ext}$ and by 16.5% in 10 mM $[Na^+]_{ext}$; it
109 similarly reduced the TaHKT1;5-D inward conductance by 57% in 1 mM $[Na^+]_{ext}$
110 and by 23% in 10 mM $[Na^+]_{ext}$ (Figs. 1 and 2). When $[Na^+]_{ext}$ was increased to 30
111 mM, the channel inwared conductance of TmHKT1;5-A was insensitive to $[K^+]_{ext}$,
112 whereas that of TaHKT1;5-D was inhibited (Fig. 2).
113
114 The increase in $[K^+]_{ext}$ from 0 to 10 mM did not significantly change the reversal
115 potential of TmHKT1;5-A or TaHKT1;5-D; all reversal potentials were close to the
116 theoretical equilibrium potential for Na^+ under all conditions (Fig. 3A, 3B).
117 Moreover, the observed shift in reversal potential were not significantly different
118 from the theoretical Nernst shift for Na^+ regardless of the presence or absence of 10
119 mM $[K^+]_{ext}$ (Fig. 3B). This suggests that neither of transporter proteins were
120 permeable to Na^+ and not to K^+.
121
122 **Dual affinity transport of Na^+ by TmHTK1;5-A and TaHKT1;5-D**
123 The affinity for Na^+ transport of TmHKT1;5-A was previously reported to be ~4-fold
124 higher than the Na^+-transport affinity of TaHKT1;5-D (4,6,19), which we confirm
125 here (Fig. 4A, 4B). On closer examination, we found a property that has not been
126 described before. When lower concentrations of $[Na^+]_{ext}$ were present it was clear that
127 the concentration dependence of inward Na^+ currents could be fitted by two
128 components, for both TmHKT1;5-A and TaHKT1;5-D (Fig. 4). For TmHKT1;5-A,
129 the high affinity component of Na^+ transport had a K_m of 18.4 μM ± 0.1 μM when
130 $[Na^+]_{ext}$ was below 0.1 mM ($K_{m\ (< 0.1\ Na)}$), whereas at concentrations of Na^+ above 0.1
131 mM the K_m was 1.0 ± 0.2 mM ($K_{m\ (> 0.1\ Na)}$) (Fig. 4A). The K_m for the higher affinity
132 component of inward Na^+ transport for TaHKT1;5-D was 15.3 μM ± 0.9 μM when
133 $[Na^+]_{ext}$ was lower than 0.1 mM ($K_{m\ (< 0.1\ Na)}$), whilst the lower affinity phase had a K_m
134 of 4.3 ± 0.5 mM when $[Na^+]_{ext}$ was higher than 0.1 mM ($K_{m\ (> 0.1\ Na)}$) (Fig. 4B).
135
136 We examined the extent of K^+-inhibition of both the lower and higher affinity
137 components of the inward Na^+ currents when $[K^+]_{ext}$ was 10 mM. The (normalised)
138 inward Na^+ current carried by both proteins was significantly suppressed by 10 mM
139 $[K^+]_{ext}$, resulting in negligible inward Na^+ transport by TmHKT1;5-A and TaHKT1;5-
140 D in presence of $[Na^+]_{ext}$ below 0.1 mM (Fig. 4C and 4D). In the presence of 10 mM

141 $[K^+]_{ext}$ it was now possible to fit the concentration dependence of inward current
142 through TmHKT1;5-A and TaHKT1;5-D with one component. The K_m values of both
143 TmHKT1;5-A and TaHKT1;5-D were decreased approximately by 2.5-fold by 10
144 mM $[K^+]_{ext}$ (Fig. 4E and 4F).
145
146 **Structural modelling of TaHKT1;5-D**
147 Three-dimensional structural models of TaHKT1;5-D were generated to explore why
148 K^+ does not traverse the pore but instead blocks the Na^+ currents, using the KtrB K^+
149 transporter from *B. subtilis* as a template (6,24). The KtrB K^+ protein was crystallised
150 in the presence of KCl, hence the original structure contained a K^+ ion in the
151 selectivity filter region. This ion was substituted by Na^+ during modelling of
152 TaHKT1;5-D as it transports Na^+ but not K^+ (6). Ramachandran analysis indicated
153 that the template and TaHKT1;5-D models generated in complex with Na^+, and K^+
154 had satisfactory stereo-chemical quality; Ramachandran plots showed only two
155 residues positioned in disallowed regions (0.5% of all residues, except glycine and
156 proline residues). Average G-factors (measures of correctness of dihedral angles and
157 main-chain covalent forces of protein molecules) calculated by PROCHECK of the
158 template and TaHKT1;5-D models with K^+ and Na^+ were 0.06. -0.18 and -0.13,
159 respectively. The ProSa 2003 analysis of z-scores (-8.4; -6.0 and -5.8) indicated that
160 template and modelled structures with K^+ and Na^+ had acceptable conformational
161 energies.
162
163 The TaHKT1;5-D model in complex with Na^+ showed that the Na^+ ion coordination
164 sphere had trigonal bipyramidal geometry, as defined by the Neighborhood algorithm
165 (25), with coordination number 5. Na^+ interacted with V76, S77, S78, N231, C232
166 and H351 (all carbonyl oxygens), that lies near the selectivity filter residues S78,
167 G233, G353 and G457 (Fig. 5A). Notably, the carbonyl oxygen one of the selectivity
168 filter residues (S78) directly participated in Na^+ binding (Fig. 5A). Conversely, the
169 TaHKT1;5-D model in complex with K^+ showed that the K^+ ion coordination sphere
170 had octahedral geometry (25) with coordination number 6; K^+ interacted with V76,
171 N231, C232, H351, N455 and V456, that were also in the close neighbour of
172 selectivity filter residues (Fig. 5B). However, in the second case, none of the
173 selectivity filter residues participate in direct binding of K^+. Ionic coordination
174 spheres and Na^+ and K^+ distances of residues were evaluated using the Metal Binding

175 Site Validation Server (25) that utilises more than 500 Protein Data Bank accession
176 numbers. Ionic coordination spheres and binding modes were found to be acceptable,
177 and ionic distances were within the following ranges: for Na^+ ranged between 2.3 and
178 2.4 Å; for K^+ were between 2.6 and 2.9 Å (Fig. 5, right panels).
179
180 **Discussion**
181 Oocytes expressing *TmHKT1;5-A* or *TaHKT1;5-D* have been previously reported to
182 undergo no obvious change in their reversal potential regardless of the presence or
183 absence of K^+ in bath solution. Interestingly, both transporters had differential
184 sensitivity to external $[K^+]_{ext}$. Whilst K^+ block occurs for TmHKT1;5-A mediating
185 inward transport it was not evident at $[Na^+]_{ext}$ above 10 mM, whereas this inhibition
186 did happen for TaHKT1;5-D up to 30 mM $[Na^+]_{ext}$ (Fig. 2) (4,19). This differential
187 inhibition effect of K^+ upon Na^+ transport at high $[Na^+]_{ext}$ by TaHKT1;5-D may result
188 from a range of factors, that govern the rates of Na^+ and K^+ ion binding and
189 subsequent Na^+ transport. A variety of factors could control the transport of Na^+ and
190 the preliminary displacement of competing K^+ with a consequent energetic cost,
191 before Na^+ passes desolvated or less-well hydrated than competing K^+. Examples
192 include free-energy variations between ions in binding sites relative to the
193 corresponding quantity in bulk water, differences in selectivity filters solvent
194 exposures (or dielectric constants), overall pore rigidity/stiffness (26), structural
195 changes within funnels and selectivity filters due to residue re-orientation, differences
196 in the hydration (coordination) numbers of Na^+ and K^+ (Na^+ and K^+ bind six and
197 seven water molecules, respectively (27)) and the alterations on the rates of Na^+ or K^+
198 de-solvation (28). It is therefore plausible to expect that both ions would compete for
199 binding sites within HKT funnel regions, yielding ion-protein binding sites with
200 differential binding strengths.
201
202 Here, we conduct advanced 3D homology modelling and include explicit ionic radii of
203 Na^+ and K^+ based on the CHARMM force field (29), rather than a traditional rigid
204 body-type modelling for ligands. The aim has been to refine the previous structural
205 model of HKT1;5 to show that the current model contains a pore that allows the
206 passage of Na^+ but not K^+ (6,10,18). This is consistent with the functional
207 observations in this and previous studies (4,19). Previously it was suggested that the
208 Gly-Gly-Gly-Gly motif is important in coordinating the K^+ ion in Ktr/TrK transporters

209 and in conferring dual Na^+-K^+ transport in HKT2 transporters (16,30). Here our
210 structural modelling suggests that the serine residue within the Ser-Gly-Gly-Gly
211 selectivity motif directly interacts and binds with Na^+ (Fig. 5B). Furthermore, our
212 model suggests, despite ionic distances being shorter for Na^+ than those for K^+, that
213 K^+ could be bound more strongly due to a higher coordination pattern (Fig. 5A and
214 5B-right panels). Obviously, during binding, K^+ takes an advantage of its larger ionic
215 radius: 152 picometer (pm), compared to that of Na^+ (116 pm); these parameters
216 reflects empirical atomic radii of K (220 pm) and Na (180 pm). We assume that under
217 the high concentrations of K^+, this ion may outcompete Na^+ and would become bound
218 in the selectivity filter, thus effectively blocking Na^+ transport. This is illustrated by
219 calculating permeation channels in both complexes, using the Mole Voronoi
220 algorithm, that predicts permeation trajectories and identifies path bottlenecks. From
221 the calculated permeation paths, it could be deduced that the K^+ ion effectively blocks
222 the permeation channel through the major gating protein pore, contrary to Na^+. It is
223 also obvious that Na^+ is likely to enter and exit the permeation trajectory from several
224 points on both sides of the transporter, but always by-passes the selectivity filter
225 constriction. Both ions arrive at the funnel of HKT proteins in solvated (hydrated)
226 forms. While the hydration number for Na^+ is 6, that for K^+ is 7 at ambient
227 temperature (27,31). The significance of the seven-fold water coordination for K^+ is
228 that this solvated complex may form a stronger hydrogen-bond interaction pattern (in
229 funnels of HKT proteins), and would be de-solvated with a higher energy input and
230 thus slower that the Na^+ solvated complex (28). It is also plausible to expect that both
231 solvated ion complexes would compete for binding sites within HKT funnel regions
232 with different binding strengths. All in all, this would contribute to the blockage of the
233 pore entry of HKT transporters by $K^{\pm}$.
234
235 Potassium permeability for HKT1 transporters has only been reported once for the
236 proteins that have been characterised in *X. laevis* oocytes. The transporters EcHKT1;1
237 and EcHKT1;2 allow permeation of both K^+ and Na^+ (15). Interestingly, when 3D
238 models of the Na^+ selective OsHKT1;5 and K^+ permeable EcHKT1;2 were
239 constructed and compared the pore size was predicted to be 0.2 Å larger in EcHKT1;2
240 (and that of OsHKT1;5 and TaHKT1;5-D), which would more than account for the
241 weaker interactions with K^+ and allow this larger ion to pass through the pore as well
242 as Na^+ (10). Without advanced 3D modelling of each and every transporter in the

243 HKT family to show how the selectivity filter forms in the context of the remainder of
244 the protein it would not be possible to predict which other HKT1s may allow passage
245 of K^+. Predictions based on sequence alone are insufficient to suggest how the two
246 sets of proteins evolved their individual Na^+ and K^+ transport characteristics. An
247 extension of the model to include other HKT proteins, a greater survey of structure-
248 function relationships and mutations of key residues to predict functionally relevant
249 residues and evolutionary relationships will be the focus of further studies.
250
251 Two affinity ranges for Na^+ transport have been detected in the HKT family
252 previously, but only for HKT2 transporters. OsHKT2;1, OsHKT2;2, OsHKT2;4 and
253 HvHKT2;1(12,13,20,32-34). For instance, for OsHKT2;2, when K^+ is present, the
254 transport of Na^+ is K^+-dependent and displays a high affinity (K_m = 0.077 mM),
255 whereas showing a lower affinity when absence of K^+ (K_m= 16 mM) (33,34).
256 OsHKT2;1 also acquires two phases of Na^+-transport affinity, whose K_m for Na^+ is
257 respectively 9.5 µM at $[Na^+]_{ext}$ below 1 mM and is 2.2 mM at $[Na^+]_{ext}$ > 1 mM (20).
258 The K^+ transport catalysed by HvHKT2;1 is affected by both $[Na^+]_{ext}$ and $[K^+]_{ext}$, such
259 as a decrease in its K^+ transport affinity from 30 µM down to 3.5 mM by $[Na^+]_{ext}$
260 increased from 0.5 mM to 30 mM and a greatly reduced channel conductivity for K^+
261 by increasing $[K^+]_{ext}$ above ~3 mM (35). This is the first time that dual affinity
262 characteristics have been reported for the HKT1;*x* family (Fig. 4). Considering the
263 relatively high homology between both clades (58% similarity/41% identity between
264 TaHKT1;5 and TaHKT2;1) it is perhaps not surprising that both clades can confer
265 dual affinity transport. How and why such ability has evolved and is conferred
266 structurally is still to be determined.
267
268 In summary, we have detected that TaHKT1;5-D and TmHKT1;5-A can both conduct
269 high and low affinity Na+ transport, both phases can be blocked by external K^+ with
270 the low affinity the low affinity component of Na^+ transport for TmHKT1;5-A being
271 less inhibited by external K^+ than TaHKT1;5-D (Fig. 4). The two K_m at the high
272 affinity phases were similar, but the K_m value for the low affinity component of
273 TmHKT1;5-A was always ~4 fold smaller regardless of the absence or presence of
274 $[K^+]_{ext}$ (Fig. 4) (4,19). TmHKT1;5-A has been shown to be more effective in
275 conferring shoot Na^+ exclusion to wheat compared to TaHKT1;5-D (36). We propose
276 that the higher affinity (with half-maximal activity nearer 1 mM compared to 4 mM),

277 and a lower sensitivity to $[K^+]_{ext}$ are both characteristics that can help confer better
278 shoot Na^+ exclusion, which is a property that can lead to greater salt tolerance in the
279 field for wheat (4,36,37).
280
281 **Materials and Methods**
282 Brief methods for cloning of *TmHKT1;5-A* and *TaHKT1;5-D* as well as its functional
283 characterisation in heterologous expression systems were described Munns et al. (4)
284 and Byrt et al. (19). Further details are included here.
285
286 **Two-electrode voltage clamp recording in *X. laevis* oocytes**
287 Oocyte recording followed the methods as described in Munns et al. (4) and Byrt et
288 al. (19). Briefly, 46 nl/23 ng of cRNA or equal volumes of RNA-free water were
289 injected into oocytes, followed by an incubation for 48 h before recording. Membrane
290 currents were recorded in the HMg solution (6 mM $MgCl_2$, 1.8 mM $CaCl_2$, 10 mM
291 MES and pH 6.5 adjusted with a TRIS base) ± Na^+ glutamate and/or K^+ glutamate as
292 indicated in relevant Figures. All solution osmolarities were adjusted using mannitol
293 at 220-240 mOsmol kg^{-1}.
294
295 **Construction of 3D models of TaHKT1;5D in complex with Na^+ and K^+ ions**
296 The most suitable template for TaHKT1;5D, the KtrB K^+ transporter from *B. subtilis*
297 (Protein Data Bank accession 4J7C, chain I) (24), was identified as previously
298 described (6). The KtrB K^+ protein was crystallised in the presence of KCl, hence the
299 structure contains a K^+ ion in the selectivity filter region. This ion was substituted by
300 Na^+ during modelling of TaHKT1;5D that transport Na^+ at a greater rate than K^+ (6).
301 3D structural models in complex with Na^+, and K^+ were generated using Modeller
302 9v16 (38) on a Linux station running the Fedora 12 operating system, as previously
303 described (6,10,18). During modelling, attention was paid to ionic radii of Na^+, and
304 K^+, whose topology parameters were taken from CHARMM (29). In each case, a total
305 of 100 models were generated that were scored by Modeller using the modeller
306 objective function (39), the discrete optimised protein energy function (40),
307 PROCHECK (41), ProSa 2003 (42) and FoldX (43). Best scoring models constructed
308 in Modeller 9v19 were further subjected to energy minimisation (knowledge-based
309 Yasara2 forcefield with parameters for bond distances, planarity of peptide bonds,
310 bond angles, Coulomb terms, dihedral angles, and van der Waals forces) (44),

311 combined with the particle-mesh-Ewald (PME) energy function for long range
312 electrostatics (cutoff 8.0 Å), to obtain smoothed electrostatic potentials. Structural
313 images were generated with PyMOL Molecular Graphics System V1.8.2.0
314 (Schrődinger LLC, Portland, OR, USA). Permeation channels and path bottlenecks in
315 both TaHKT1;5D ionic complexes were calculated using the Mole algorithm,
316 embedded in PyMol (45), but using the x-y-z coordinates of Na^+ or K^+ as
317 specifications for starting points.
318

319 **Funding**
320 This work was supported by funding to M.G. from the Grains Research and
321 Development Corporation (UA00145), the Australian Research Council through the
322 Centre of Excellence (CE1400008) and Future Fellowship (FT130100709) schemes,
323 and by funding to M.H. from the Australian Research Council (DP120100900).
324

325 **References**

326 1. Munns, R., and Tester, M. (2008) Mechanisms of salinity tolerance. *Annu.*
327 *Rev. Plant Biol.* **59**, 651-681
328 2. Ren, Z.-H., Gao, J.-P., Li, L.-G., Cai, X.-L., Huang, W., Chao, D.-Y., Zhu,
329 M.-Z., Wang, Z.-Y., Luan, S., and Lin, H.-X. (2005) A rice quantitative trait
330 locus for salt tolerance encodes a sodium transporter. *Nat. Genet.* **37**, 1141-
331 1146
332 3. James, R. A., Davenport, R. J., and Munns, R. (2006) Physiological
333 characterization of two genes for Na^+ exclusion in durum wheat, *Nax1* and
334 *Nax2*. *Plant Physiol.* **142**, 1537-1547
335 4. Munns, R., James, R. A., Xu, B., Athman, A., Conn, S. J., Jordans, C., Byrt,
336 C. S., Hare, R. A., Tyerman, S. D., Tester, M., Plett, D., and Gilliham, M.
337 (2012) Wheat grain yield on saline soils is improved by an ancestral Na^+
338 transporter gene. *Nat. Biotech.* **30**, 360-364
339 5. Campbell, M. T., Bandillo, N., Al Shiblawi, F. R. A., Sharma, S., Liu, K., Du,
340 Q., Schmitz, A. J., Zhang, C., Véry, A.-A., and Lorenz, A. J. (2017) Allelic
341 variants of OsHKT1; 1 underlie the divergence between indica and japonica
342 subspecies of rice (*Oryza sativa*) for root sodium content. *PLoS Genet.* **13**,
343 e1006823
344 6. Xu, B., Waters, S., Byrt, C. S., Plett, D., Tyerman, S. D., Tester, M., Munns,
345 R., Hrmova, M., and Gilliham, M. (2018) Structural variations in wheat
346 HKT1; 5 underpin differences in Na^+ transport capacity. *Cell. Mol. Life Sci.*,
347 1-12
348 7. Sentenac, H., and Bonneaud, N. (1992) Cloning and expression in yeast of a
349 plant potassium ion transport system. *Science* **256**, 663
350 8. Corratgé-Faillie, C., Jabnoune, M., Zimmermann, S., Véry, A.-A., Fizames,
351 C., and Sentenac, H. (2010) Potassium and sodium transport in non-animal
352 cells: the Trk/Ktr/HKT transporter family. *Cell. Mol. Life Sci.* **67**, 2511-2532

9. Asins, M. J., Villalta, I., Aly, M. M., Olias, R., Álvarez De Morales, P., Huertas, R., Li, J., JAIME-PÉREZ, N., Haro, R., and Raga, V. (2013) Two closely linked tomato HKT coding genes are positional candidates for the major tomato QTL involved in Na^+/K^+ homeostasis. *Plant Cell Environ.* **36**, 1171-1191
10. Waters, S., Gilliham, M., and Hrmova, M. (2013) Plant high-affinity potassium (HKT) transporters involved in salinity tolerance: structural insights to probe differences in ion selectivity. *Int. J. Mol. Sci.* **14**, 7660-7680
11. Lan, W.-Z., Wang, W., Wang, S.-M., Li, L.-G., Buchanan, B. B., Lin, H.-X., Gao, J.-P., and Luan, S. (2010) A rice high-affinity potassium transporter (HKT) conceals a calcium-permeable cation channel. *Proc. Natl. Acad. Sci. U.S.A.* **107**, 7089-7094
12. Horie, T., Brodsky, D. E., Costa, A., Kaneko, T., Schiavo, F. L., Katsuhara, M., and Schroeder, J. I. (2011) K^+ transport by the OsHKT2; 4 transporter from rice with atypical Na^+ transport properties and competition in permeation of K^+ over Mg^{2+} and Ca^{2+} ions. *Plant Physiol.* **156**, 1493-1507
13. Sassi, A., Mieulet, D., Khan, I., Moreau, B., Gaillard, I., Sentenac, H., and Véry, A.-A. (2012) The rice monovalent cation transporter OsHKT2; 4: revisited ionic selectivity. *Plant Physiol.* **160**, 498-510
14. Uozumi, N., Kim, E. J., Rubio, F., Yamaguchi, T., Muto, S., Tsuboi, A., Bakker, E. P., Nakamura, T., and Schroeder, J. I. (2000) The Arabidopsis HKT1 gene homolog mediates inward Na^+ currents in *Xenopus laevis* oocytes and Na^+ uptake in *Saccharomyces cerevisiae*. *Plant Physiol.* **122**, 1249-1260
15. Liu, W., Fairbairn, D. J., Reid, R. J., and Schachtman, D. P. (2001) Characterization of two HKT1 homologues from *Eucalyptus camaldulensis* that display intrinsic osmosensing capability. *Plant Physiol.* **127**, 283-294
16. Mäser, P., Hosoo, Y., Goshima, S., Horie, T., Eckelman, B., Yamada, K., Yoshida, K., Bakker, E. P., Shinmyo, A., and Oiki, S. (2002) Glycine residues in potassium channel-like selectivity filters determine potassium selectivity in four-loop-per-subunit HKT transporters from plants. *Proc. Natl. Acad. Sci. U.S.A.* **99**, 6428-6433
17. Platten, J. D., Cotsaftis, O., Berthomieu, P., Bohnert, H., Davenport, R. J., Fairbairn, D. J., Horie, T., Leigh, R. A., Lin, H.-X., and Luan, S. (2006) Nomenclature for HKT transporters, key determinants of plant salinity tolerance. *Trends Plant Sci.* **11**, 372-374
18. Cotsaftis, O., Plett, D., Shirley, N., Tester, M., and Hrmova, M. (2012) A two-staged model of Na^+ exclusion in rice explained by 3D modeling of HKT transporters and alternative splicing. *PLoS One* **7**, e39865
19. Byrt, C. S., Xu, B., Krishnan, M., Lightfoot, D. J., Athman, A., Jacobs, A. K., Watson-Haigh, N. S., Plett, D., Munns, R., and Tester, M. (2014) The Na^+ transporter, TaHKT1;5-D, limits shoot Na^+ accumulation in bread wheat. *Plant J.* **80**, 516-526
20. Jabnoune, M., Espeout, S., Mieulet, D., Fizames, C., Verdeil, J.-L., Conéjéro, G., Rodríguez-Navarro, A., Sentenac, H., Guiderdoni, E., and Abdelly, C. (2009) Diversity in expression patterns and functional properties in the rice HKT transporter family. *Plant Physiol.* **150**, 1955-1971
21. Almeida, P., de Boer, G.-J., and de Boer, A. H. (2014) Differences in shoot Na^+ accumulation between two tomato species are due to differences in ion affinity of HKT1;2. *J. Plant Physiol.* **171**, 438-447

402 22. Almeida, P., Feron, R., de Boer, G.-J., and de Boer, A. H. (2014) Role of Na^+,
403 K^+, Cl^-, proline and sucrose concentrations in determining salinity tolerance
404 and their correlation with the expression of multiple genes in tomato. *AoB*
405 *Plants* **6**, plu039
406 23. Ben Amar, S., Brini, F., Sentenac, H., Masmoudi, K., and Véry, A.-A. (2013)
407 Functional characterization in *Xenopus oocytes* of Na^+ transport systems from
408 durum wheat reveals diversity among two HKT1; 4 transporters. *J. Exp. Bot.*
409 **65**, 213-222
410 24. Vieira-Pires, R. S., Szollosi, A., and Morais-Cabral, J. H. (2013) The structure
411 of the KtrAB potassium transporter. *Nature* **496**, 323-328
412 25. Zheng, H., Chordia, M. D., Cooper, D. R., Chruszcz, M., Müller, P.,
413 Sheldrick, G. M., and Minor, W. (2014) Validation of metal-binding sites in
414 macromolecular structures with the CheckMyMetal web server. *Nat. Protoc.*
415 **9**, 156
416 26. Dudev, T., and Lim, C. (2010) Factors governing the Na^+ vs K^+ selectivity in
417 sodium ion channels. *J. Am. Chem. Soc.* **132**, 2321-2332
418 27. Rowley, C. N., and Roux, B. t. (2012) The solvation structure of Na^+ and K^+
419 in liquid water determined from high level ab initio molecular dynamics
420 simulations. *J. Chem. Theory Comput.* **8**, 3526-3535
421 28. Degrève, L., Vechi, S. M., and Junior, C. Q. (1996) The hydration structure of
422 the Na^+ and K^+ ions and the selectivity of their ionic channels. *Biochim.*
423 *Biophys. Acta-Bioenergetics* **1274**, 149-156
424 29. Brooks, B. R., Brooks, C. L., MacKerell, A. D., Nilsson, L., Petrella, R. J.,
425 Roux, B., Won, Y., Archontis, G., Bartels, C., and Boresch, S. (2009)
426 CHARMM: the biomolecular simulation program. *Journal of Computational*
427 *Chemistry* **30**, 1545-1614
428 30. Durell, S. R., and Guy, H. R. (1999) Structural models of the KtrB, TrkH, and
429 Trk1, 2 symporters based on the structure of the KcsA K^+ channel. *Biophys. J.*
430 **77**, 789-807
431 31. Ma, H. (2014) Hydration structure of Na^+, K^+, F^-, and Cl^- in ambient and
432 supercritical water: A quantum mechanics/molecular mechanics study. *Int. J.*
433 *Quantum Chem.* **114**, 1006-1011
434 32. Schachtman, D. P., and Schroeder, J. I. (1994) Structure and transport
435 mechanism of a high-affinity potassium uptake transporter from higher plants.
436 *Nature* **370**, 655-658
437 33. Rubio, F., Gassmann, W., and Schroeder, J. I. (1995) Sodium-driven
438 potassium uptake by the plant potassium transporter HKT1 and mutations
439 conferring salt tolerance. *Science* **270**, 1660
440 34. Yao, X., Horie, T., Xue, S., Leung, H.-Y., Katsuhara, M., Brodsky, D. E., Wu,
441 Y., and Schroeder, J. I. (2010) Differential sodium and potassium transport
442 selectivities of the rice OsHKT2; 1 and OsHKT2; 2 transporters in plant cells.
443 *Plant Physiol.* **152**, 341-355
444 35. Mian, A., Oomen, R. J., Isayenkov, S., Sentenac, H., Maathuis, F. J., and
445 Véry, A. A. (2011) Over-expression of an Na^+-and K^+-permeable HKT
446 transporter in barley improves salt tolerance. *Plant J.* **68**, 468-479
447 36. James, R. A., Blake, C., Zwart, A. B., Hare, R. A., Rathjen, A. J., and Munns,
448 R. (2012) Impact of ancestral wheat sodium exclusion genes *Nax1* and *Nax2*
449 on grain yield of durum wheat on saline soils. *Funct. Plant Biol.* **39**, 609-618
450 37. James, R. A., Blake, C., Byrt, C. S., and Munns, R. (2011) Major genes for
451 Na^+ exclusion, *Nax1* and *Nax2* (wheat *HKT1; 4* and *HKT1; 5*), decrease Na+

452 accumulation in bread wheat leaves under saline and waterlogged conditions.
453 *J. Exp. Bot.* **62**, 2939-2947
454 38. Šali, A., and Blundell, T. L. (1993) Comparative protein modelling by
455 satisfaction of spatial restraints. *J. Mol. Biol.* **234**, 779-815
456 39. Shen, M. y., and Sali, A. (2006) Statistical potential for assessment and
457 prediction of protein structures. *Protein Sci.* **15**, 2507-2524
458 40. Eswar, N., Eramian, D., Webb, B., Shen, M.-Y., and Sali, A. (2008) Protein
459 structure modeling with MODELLER. in *Structural proteomics*, Springer. pp
460 145-159
461 41. Laskowski, R. A., MacArthur, M. W., Moss, D. S., and Thornton, J. M. (1993)
462 PROCHECK: a program to check the stereochemical quality of protein
463 structures. *J. Appl. Crystallogr.* **26**, 283-291
464 42. Sippl, M. J. (1993) Recognition of errors in three-dimensional structures of
465 proteins. *Proteins: Struct., Funct., Bioinf.* **17**, 355-362
466 43. Schymkowitz, J., Borg, J., Stricher, F., Nys, R., Rousseau, F., and Serrano, L.
467 (2005) The FoldX web server: an online force field. *Nucleic Acids Res.* **33**,
468 W382-W388
469 44. Krieger, E., Darden, T., Nabuurs, S. B., Finkelstein, A., and Vriend, G. (2004)
470 Making optimal use of empirical energy functions: force-field
471 parameterization in crystal space. *Proteins: Struct., Funct., Bioinf.* **57**, 678-
472 683
473 45. Petřek, M., Košinová, P., Koča, J., and Otyepka, M. (2007) MOLE: a Voronoi
474 diagram-based explorer of molecular channels, pores, and tunnels. *Structure*
475 **15**, 1357-1363
476

477

478 **Figures and figure legends**

479 **Figure 1. K^+-sensitivity of Na^+ currents carried by TmHKT1;5-A and**
480 **TaHKT1;5-D.** A-D, current-voltage (I/V) curves of Na^+ currents recorded from *X.*
481 *laevis* oocytes expressing *TmHKT1*;5-*A* (A, C) and *TaHKT1*;5-*D* (B, D) in 1 mM Na^+
482 plus 0-30 mM K^+ (A,B), or 0-30 mM Na^+ solutions with or without 10 mM K^+ (C,D).
483 Mean ± S.E.M, n = 5-6.
484

485 **Figure 2. Channel conductance of TmHKT1;5-A and TaHKT1;5-D.** The channel
486 conductance of TmHKT1;5-A and TaHKT1;5-D was calculated from Figure 1, based
487 on the slope of curve between -140 mV and -120 mV, statistical difference was
488 determined by *Students' t-test*, $*P < 0.05$ and $** P < 0.01$.
489

490 **Figure 3. Shift in reversal potential of TmHKT1;5-A and TaHKT1;5-D in**
491 **response to changes in $[Na^+]_{ext}$ and $[K^+]_{ext}$.**
492 A, Reversal potential of currents in *X. laevis* oocytes expressing *TmHKT1*;5-*A* (red)
493 and *TaHKT1*;5-*D* (blue) derived from Figure. 1. B, Reversal potential of Na^+ currents
494 plotted with theoretical Nernst potential derived from internal concentrations
495 measured in Munns et al. (2012) [19] and Byrt et al., (2014) [4]. Voltage at which
496 current reversed in oocytes expressing *TmHKT1*;5-*A* and *TaHKT1*;5-*D* in solutions
497 containing 1 mM to 10 mM Na^+ ($[1\text{-}10]_{ext}$ Na^+) and 10 mM to 30 mM Na^+ ($[10\text{-}30]_{ext}$
498 Na^+) with or without 10 mM $[K^+]_{ext}$, ΔV_{Na} of 0 mM or 10 mM K^+ = experimentally
499 measured shift in reversal potential for Na^+ in 0 mM or 10 mM K^+ conditions as
500 indicated; ΔV_{Na} of E_{Na} = theoretical equilibrium (or Nernst) potential for Na^+ was
501 57.7 mV and 26.9 mV, respectively for $[1\text{-}10]_{ext}$ Na^+ and $[10\text{-}30]_{ext}$ Na^+. One way
502 ANOVA was performed for Figure 3B and no statistical differences were found
503 between the theoretical and experimentally measured values.
504

505 **Figure 4. Transport affinity of TmHKT1;5-A and TaHKT1;5-D in *X. laevis***
506 **oocytes.**
507 A-B, dual Na^+-transport affinity of TmHKT1;5-A and TaHKT1;5-D in *X. laevis*
508 oocytes, plotted as normalised currents at -140 mV as shown against a series of Na^+
509 glutamate solutions. C-D, high affinity phase of TmHKT1;5-A and TaHKT1;5-D in
510 absence and presence of 10 mM $[K^+]_{ext}$. Data represented in A, B and C as mean ±
511 S.E.M (n = 4 for A, n = 7 for B, n = 4 of 0 mM K^+ and n = 5 of 10 mM K^+ for C). E-

512 F, Na^+-transport affinity of TmHKT1;5-A and TaHKT1;5-D in *X. laevis* oocytes,
513 plotted as normalised currents at -140 mV as shown against a series of Na^+ glutamate
514 solutions with an additional 10 mM K^+ glutamate, n = 5 for E and n = 4 for F.
515
516 **Figure 5. Molecular models of TaHKT1;5D in complex with Na^+ (A) and K^+ (B)**
517 **ions.**

518 **(A-B; left panels)** Cartoon representations of TaHKT1;5-D illustrate overall protein
519 folds with cylindrical α-helices, and translocating permeation channels (black mesh).
520 Na^+ (A) and K^+ (B) ions are shown as purple spheres located within the selectivity
521 filter residues S78, G233, G353 and G457 (coloured in cpk magenta), and other
522 neighbouring residues. Na^+ is likely to enter and exit the permeation trajectory from
523 several points on both sides of the transporter, but always by-passes the selectivity
524 filter constriction. K^+ enters the selectivity filter and effectively blocks the permeation
525 at the constriction bottleneck. For clarity, membrane α-helices are only shown.

526 **(A-B; right panels)** Detailed views of coordination spheres of Na^+ and K^+ ions, and
527 ionic interactions with residues adjoining the selectivity filter residues S78, G233,
528 G353 and G457. The ionic distances of 2.3-2.8 Å for Na^+ between V76, S77, S78,
529 N231, C232 and H351, and of 2.6-2.9 Å for K^+ between V76, N231, C232, H351,
530 N455 and V456, are formed between carbonyl oxygens of residues (in sticks in atomic
531 colours). The K^+ ion effectively blocks the permeation channel through the protein
532 pore at the constriction bottleneck point, contrary to Na^+.
533

534 **Figure 1**

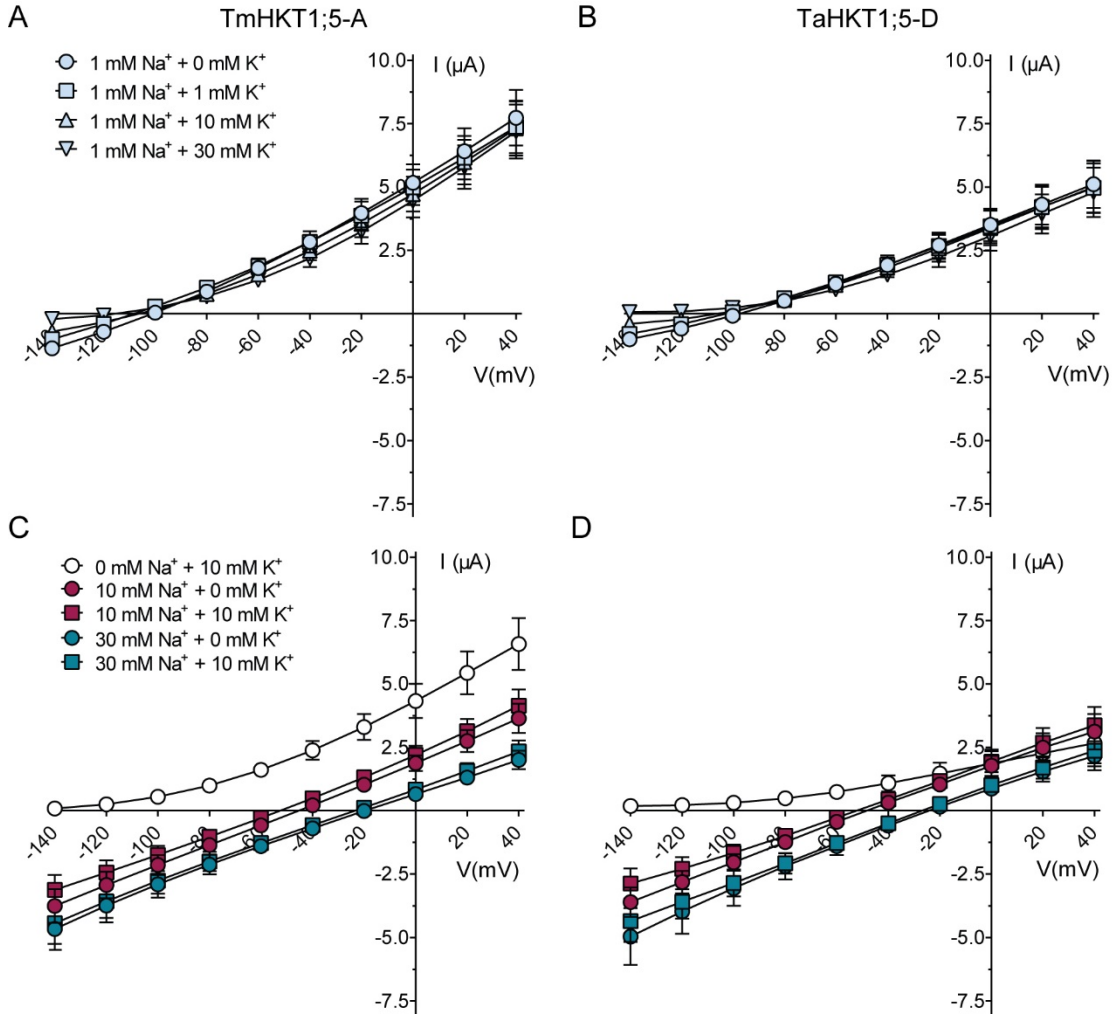

535

536

537

538 **Figure 2**

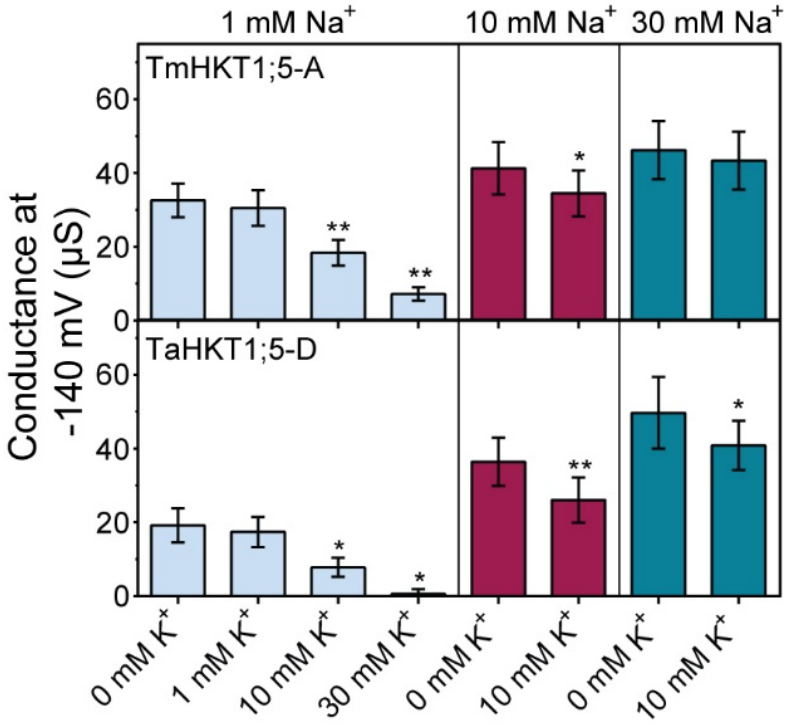

539

540

541 **Figure 3**

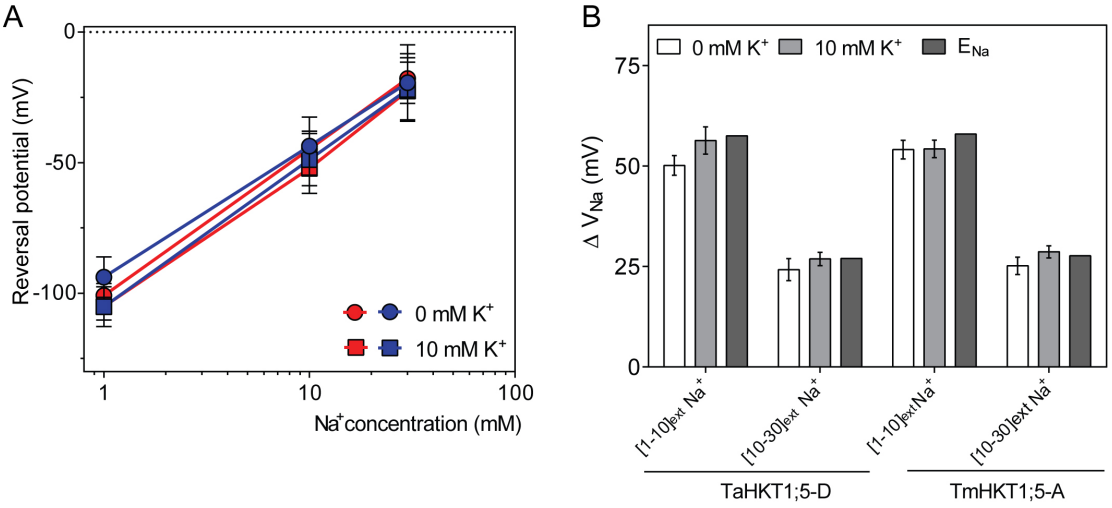

542

543

544 **Figure 4**

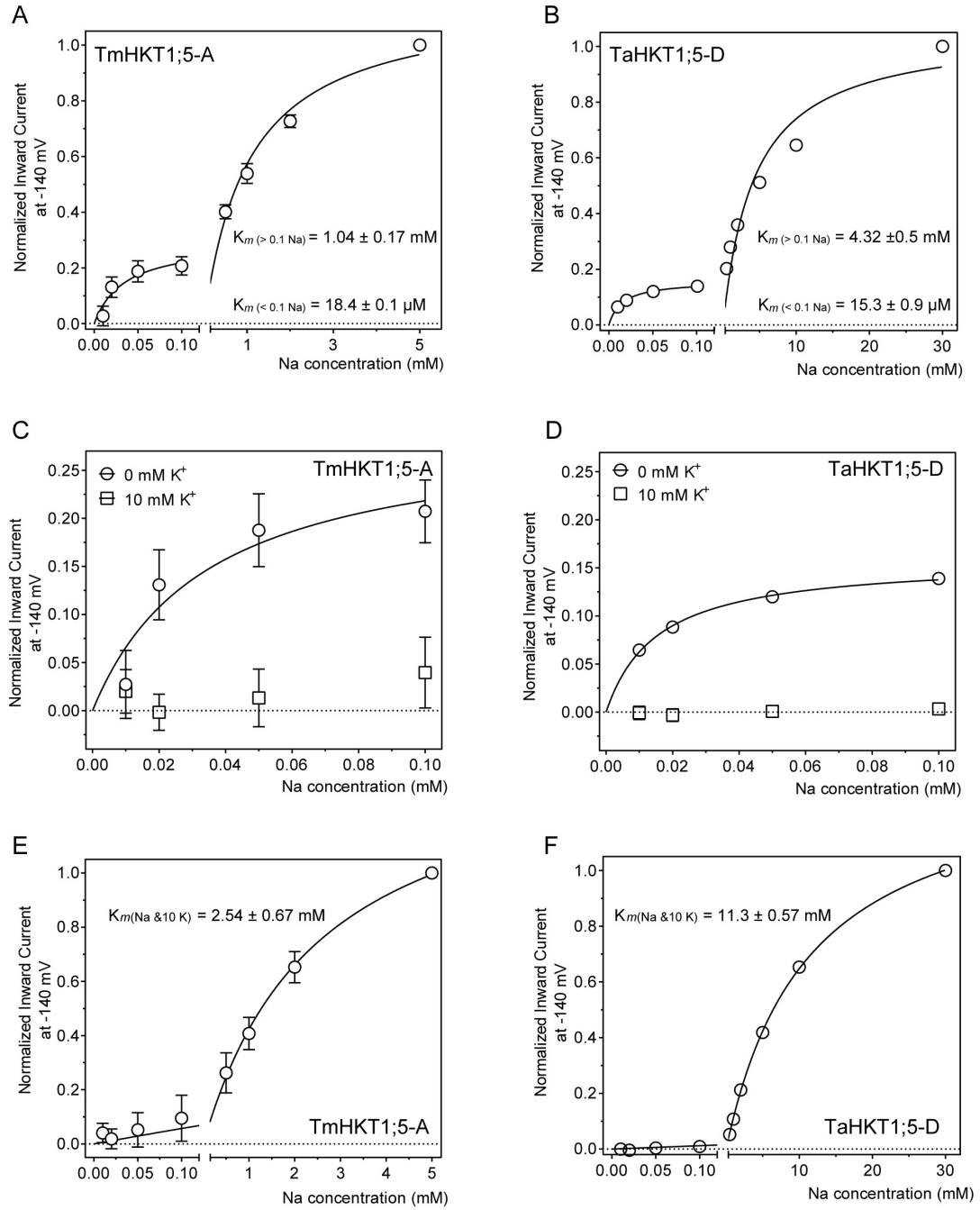

545

546

547

548 **Figure 5**

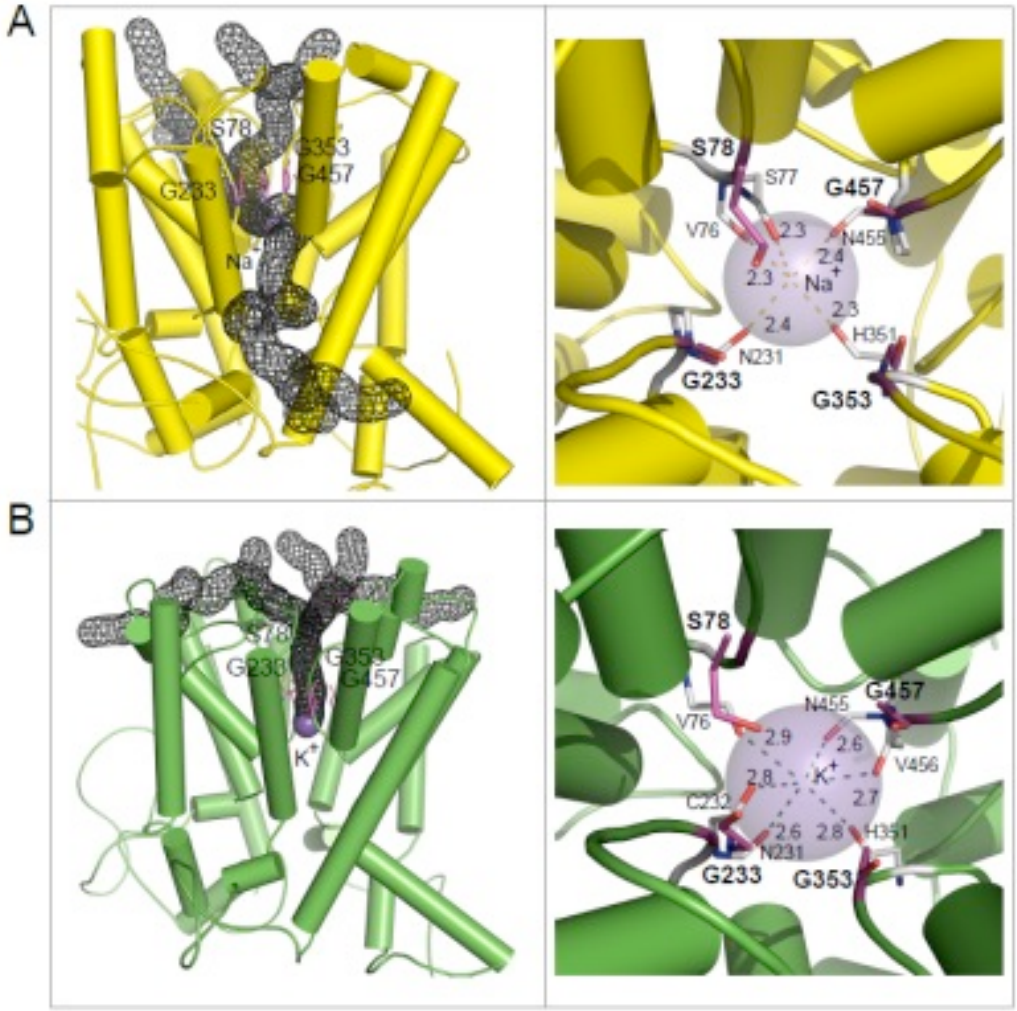

549
550

551